DIABATIC FLOWS ON ELECTRICALLY-DRIVEN RADIAL MICRO-TURBOCOMPRESSORS

Andrés Sebastián, Rubén Abbas, Manuel Valdés*

Universidad Politécnica de Madrid (UPM)
José Gutiérrez Abascal 2, 28006 Madrid (Spain)
*andres.sebastian@upm.es

ABSTRACT

Radial compressors miniaturization entails diverse challenging aerothermal effects on their performance. Among them, an immediate downsizing-related issue comes along in the field of heat transfer because these reduced-scale machines cannot be treated as adiabatic. Resultant specific heat losses are indeed high enough to be necessarily taken into account. Furthermore, novel proposals for using electric drive technologies instead of conventional directly-coupled turbines include some particularities on their thermal behavior assessment. This is precisely why this work is focused on identifying the key underlying heat transfer mechanisms when the micro-compressor is running under diabatic conditions. The numerical results show how the diffuser and the volute provide the largest impact on the flow when dealing with diabatic walls while inlet and impeller domains provide a considerably lower impact. This finding allows the proposal of straightforward correction methods in experimentation for these diabatic flows considering compressor outlet flow properties.

KEYWORDS

MICRO-TURBOMACHINERY, DIABATIC COMPRESSION, HEAT TRANSFER, NON-ADIABATICITY

NOMENCLATURE

A	Area (m^2)		**Subscripts**
c_p	Specific heat capacity (J/kgK)	$0a$	ambient
GCI	Grid convergence index (-)	$0i$	impeller axis
$\dot{m}$	Mass flow (kg/s)	1	inlet
Nu	Nusselt number (-)	2	impeller
$\dot{Q}$	Heat flow (W)	3	diffuser
q	Specific heat flow (kJ/kg)	4	volute
Re	Reynolds number (-)	b	blade
T	Temperature (°C)	c	coolant
u^*	Dimensionless velocity (-)	h	hub
η_p	Polytropic efficiency (-)	m	motor
π	Total-to-total pressure ratio (-)	s	shroud
ρ	Density (kg/m^3)	w	wall

INTRODUCTION

Miniaturized turbocompressors arise as a promising technology which can be part of novel environmentally friendly systems. Apart from power and propulsion applications, such as green microturbines or fuel cells turbocharging, novel proposals are also conceived for the heating and cooling sector with increased-efficiency heat pumps or renewable micro-trigeneration systems using working fluids other than air (Sebastián et al., 2021c). These miniature radial compressors (also referred as millimeter-size radial compressors or simply micro-compressors) are classified according to Casey et al. (2013) for having impeller outer diameters less than 30 mm and rotational speeds greater than 200 $kmin^{-1}$. Their applicability has notably boosted owing to the development of gas lubricated bearing technologies and ultra-high-speed electric motors. Among all the different electric drive technologies, permanent magnet synchronous machines offer the highest power density while reaching the highest rotational speeds (Tüysüz et al., 2015).

The main flow heat loss is a performance-limiting factor identified when conceiving miniaturized radial compressors. Gong et al. (2004) stated that the resultant high surface-to-flow ratio arising from miniaturization has the consequence that the flow in the micro-compressor can no longer be taken as adiabatic. Therefore, an external heat addition/removal must be considered to predict this non-adiabatic behavior (Sirakov, 2005). Apart from degrading the micro-compressor performance, the experimental characterization of its actual internal efficiency is hindered due to the distortion generated in the measurements of the flow.

The closeness between the turbine and the compressor coupling in micro gas turbines or in automotive turbochargers conveys large heat flows from the hot side (turbine) to the cold side (compressor). This has led to the analysis and optimization of the entire assembly to include the heat transfer phenomena in the global performance of the system (Van den Braembussche et al., 2003). Casey and Fesich (2010) presented the advantages of using a polytropic approach for determining the compressors actual efficiency when dealing with diabatic flows. This view was widely accepted by the academic community. For instance, the study of Verstraete and Hewakuruppu (2012) presented the adaptation of a 1D design and performance analysis code to accommodate these heat transfer effects. The impact of the non-adiabatic behavior of the micro-scale compressor main flow field was also deeply studied by CFD simulations (Sun et al., 2014). Finally, empirical-based correction methodologies have been raised to predict heat transfer coefficients and diabatic flows in small turbochargers (Serrano et al., 2015; Savic et al., 2017).

Nevertheless, the proposal of electric drive technologies instead of turbines conveys some specificities which need to be analyzed to assess the electric micro-turbocompressor thermal behavior. The use of directly-coupled turbines implied a large temperature difference which leads to an easier determination of the representative heat flow. Electric motors thermal behavior, instead, mainly depends on the winding temperature which needs to be limited to prevent any damages to the motor. Therefore, active or passive cooling methods are required to limit these temperature values originating smaller diabatic flows which need to be characterized.

The goal of this work is to identify the heat flow distribution on a micro-compressor when its wall temperature is indirectly controlled to ensure a proper operation of the motor. For this purpose, a numerical model of a complete radial compressor stage has been used to compare and analyze its adiabatic and diabatic performance using both a gas (air) and a vapor (propane) at similarity conditions. This study contributes to a better understanding of the compressor diabatic behavior at small scale. Hence, results of this work have been applied to develop reduced-order heat transfer correction methods necessary to experimentally characterize an electrically-driven micro-scale radial compressor (Sebastián et al., 2023).

NON-ADIABATICITY AND HEAT FLOWS IDENTIFICATION

The classical approach of adiabatic flow in non-refrigerated turbomachinery is quite common because of their large size and their corresponding high mass flow. Nevertheless, the size reduction of miniaturized turbomachinery conveys an increase in the surface-to-flow ratio of the machine. Heat flows are proportional to the transmission area where are considered; besides, the mass flow is proportional to the cross-section area and the inlet velocity, which in turn is also related to the diameter-dependent peripheral speed. Thus, the heat transferred is proportional to the square of the characteristic length of the machine while the mass flow is proportional to the cube. This is why the characteristic size of the machine has a crucial impact on the effect of external heat flows ruled by an inversely proportional relationship.

As a result, a convective heat flow caused by the temperature difference between the walls and the free-stream flow occurs. This temperature gradient can be produced by means of different mechanisms: (i) internal conduction over the entire hub/shroud from the hot to the cold side of the turbomachine; (ii) heat losses to the ambient; (iii) external heat flows from adjacent heat sources such as lubricating oil, water cooling or the hot side of a turbine or, in this case, an electric motor. The distribution of the resultant temperature gradient on the walls will depend on the thermal conductivity of the material and the wall thickness. Hence, a temperature mapping of the entire machine would be necessary in order to characterize properly the three-dimensional heat fluxes.

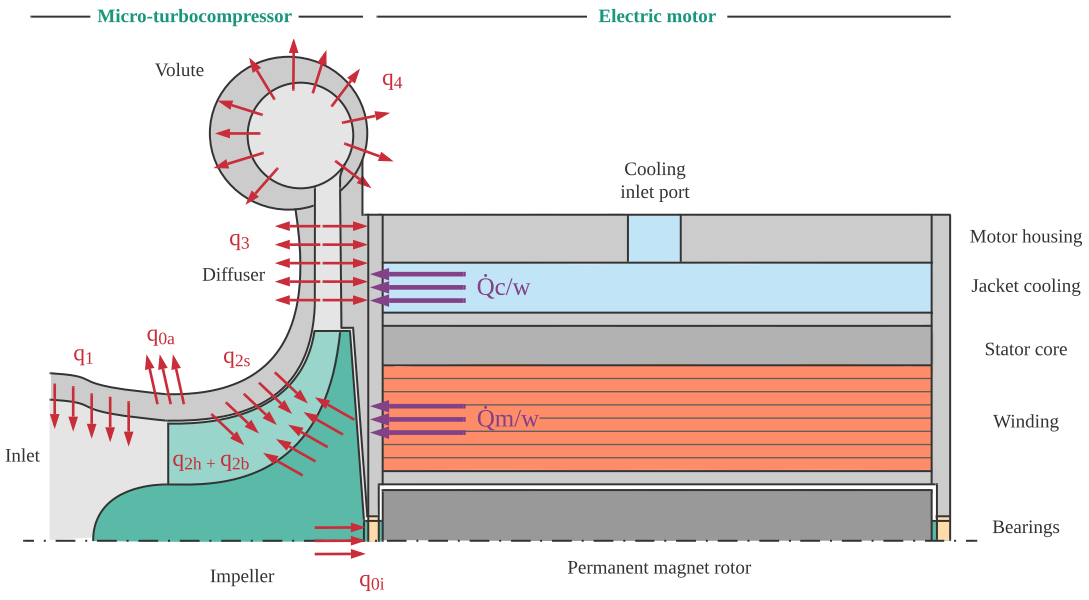

Figure 1: **Illustrative diagram of the different heat flows on a water-cooled and electrically-driven micro-turbocompressor.**

Figure 1 shows a schematic diagram of a micro-turbocompressor coupled to a water-cooled electric motor (PMSM) with a jacket cooling around the stator. As previously mentioned, the electric motor operation necessarily involves a temperature increase due to the circulating current across its winding. This heat source is controlled by means of an external active cooling. This involves two external heat flows due to the close proximity of the motor: the heat flux from

the motor to the compressor wall $\dot{Q}_{m/w}$ and the heat flux from the cooling to the compressor wall as a side effect due to the necessary motor cooling $\dot{Q}_{c/w}$. Both external heat sinks/sources induce an unavoidable variation of the wall/casing temperature.

On the micro-turbocompresor side, four different heat fluxes to the flow field can be identified in a diabatic compression: q_1 at the inlet, q_2 at the impeller, q_3 at the diffuser and q_4 along the volute. These fluxes have been represented in a meridional view in Figure 1. In addition, external heat fluxes (q_0) along the impeller axis (q_{0i}) and to the ambient (q_{0a}) are also represented. The former can be of significant relevance if there are adjacent heat sinks/sources. The latter can be usually neglected if a proper insulation of the cover is guaranteed. One may recall that the compressors operating temperature range is low enough to neglect radiation heat transfer.

The first heat flux (q_1) considers the heat exchange from the inlet duct walls. The heating of these walls is due to the internal conduction of the cover from the hot to the cold side. This situation may lead to a pre-heating of the flow field before entering the impeller. The second heat flow considered is around the impeller region (q_2), which includes the blades (q_{2b}), the hub (q_{2h}) and the shroud (q_{2s}). The origin of this later flux is similar to q_1, but with a smoother temperature gradient instead. Regarding the fluxes at the impeller walls, a temperature gradient may exist by means of conduction along the impeller axis. This axis could be coupled, for instance, to an electric motor or a turbine. Consequently, both drivers can reject heat by means of this mechanism. The third one is the heat transfer through the diffuser walls (q_3). Here, the temperature of the working fluid has been increased because of the pressure rise across the impeller. Therefore, the fluid would be at a higher temperature than the walls which would lead to a cooling process. However, this heat flux can be altered if there is an adjacent system coupled to the compressor. If a water-cooled electric motor is the driver of the compressor, the water cooling temperature will heat/cool the compressor walls at this point. The last heat flux considered is the one from the volute walls (q_4) which has a similar origin than q_3 and could be altered in the same way by an external heat source/sink. Although the fluid flows have lower velocities in the volute than along the impeller, the increased surface of the volute will have an important impact on the fluid.

A net heat flux to/from the flow field can be assessed by means of computing all these heat fluxes, which could entail a heat addition ($q > 0$) or a heat removal ($q < 0$). The relative importance of the underlying mechanism of each heat flux may convey consequently to different scenarios. This is precisely why the distribution of these heat fluxes is assessed in this work.

NUMERICAL MODEL AND METHODS

A closer look to the micro-compressor non-adiabaticity can be taken by means of CFD simulations. A three-dimensional numerical model can provide valuable information about the heat flux distribution along the micro-compressor apart from its influence on the global performance. The numerical model used for this analysis is based on the micro-scale radial compressor model developed in Sebastián et al. (2021a,b) using ANSYS CFX. It is a one-stage centrifugal compressor consisting of a 20 mm impeller with seven blades and seven splitter blades rotating at 220 kmin^{-1} at design conditions and a vaneless diffuser. The micro-compressor provides an overall pressure ratio around 1.4 consuming 330 W. To perform a stationary thermal analysis, an additional volute model is coupled to the reference stage using the frozen rotor approach because of the non-axisymmetric volute flow domain. The outlet boundary condition is consequently moved downstream to the volute outlet, setting the mass flow rate, while inlet conditions define total temperature and pressure.

The mesh of the volute domain is composed of approximately 19.7 million cells. Due to its non-symmetrical geometry, this domain requires to be simulated on its entire geometry. The resultant mesh is based of unstructured tetrahedrons with additional inflation layers on the wall surfaces. Regarding the quality of the tetrahedral mesh, the maximum skewness is maintained below 0.9 with an average skewness of 0.2. Aspect ratio and smoothness requirements are consequently also fulfilled. The mesh on the volute domain is depicted in Figure 2.

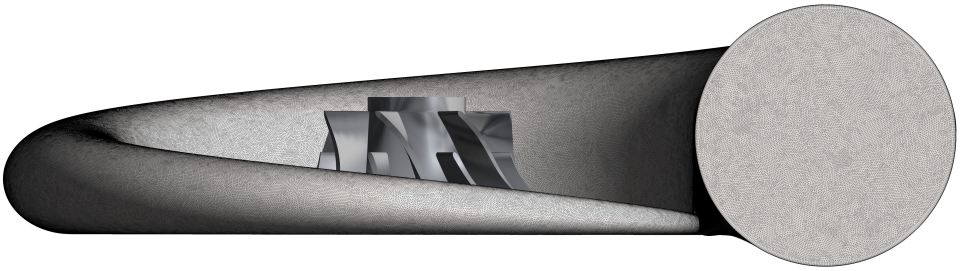

Figure 2: **Illustrative view of the reference micro-scale compressor full model including the meshed fluid domain of the volute.**

Mesh independent results in CFD can be guaranteed following the procedure proposed by Celik et al. (2008) based on the Richardson extrapolation. This method provides a Grid Convergence Index (GCI), which is one of the most recognized parameters to determine the error band on the grid convergence solution (discretization error). Taking the reference volute mesh of 19.7 million cells with an average cell size of 0.089 mm, two additional meshes have been studied. The first one is the coarse mesh with 8.8 million cells, whereas 43.7 million cells are required in the fine mesh. The convective heat flux on the volute walls has been the key parameter selected for the volute model due to its important role for characterizing the heat transfer phenomena dealing with diabatic flows. The GCI from the fine grid to the intermediate (GCI_{12}) value obtained is 0.07%, well below the GCI from the intermediate to the coarse mesh GCI_{23} (0.72%), which allow the use of the reference mesh for each numerical problem ensuring stable and grid-insensitive results.

As it has been discussed in the previous section, there are many factors which can origin a temperature gradient on the compressor casing/walls. It is clear that there will be a temperature distribution on the walls instead of a constant profile because the casing material is thermally conductive (i.e. aluminum). Nevertheless, this study will consider a constant temperature on all the considered walls in order to carry on a simplified analysis of the heat fluxes distribution. This conservative assumption sets a wall temperature at the mean compressor inlet-outlet fluid temperature. The calculation of these heat fluxes in the complete numerical model will be addressed by means of Equation 1, which holds the integration of the heat flux on each node over the entire surface. The heat flux is modeled using the thermal law of the wall function of Kader (1981) in the thermal boundary layer. It provides the non-dimensional temperature (T^+) distribution by blending the viscous sublayer an the logarithmic law of the wall, ruled by the dimensionless velocity u^*. This method is recommended by the CFX solver when dealing with the automatic wall function approach with the k-ω turbulence model.

$$q = \frac{1}{\dot{m}} \int q_w dA = \frac{1}{\dot{m}} \int \frac{\rho c_p u^*}{T^+} (T_w - T) dA \tag{1}$$

As previously introduced, the goal of the study is to analyze the distribution and impact of the the diabatic performance of an electrically-driven micro-turbocompressor. Apart from its design and off-design performance using air, the same geometry will be simulated using a vapor-like working fluid (propane) under dynamic similarity conditions due to the increased interest in small turbomachinery using non-ideal working fluids. The similitude-based pseudo-homologous transformation (Sebastián et al., 2021a) has been used to determine these equivalent operating points. Apart from fulfilling dynamical similarity conditions among them, Reynolds-number-dependent viscous effects are also considered since the small scale of the compressor leads to a transitional laminar-to-turbulent flow regime operation. Hence, this comparison will show also the the size effect – by means of increasing the Reynolds number (Re) – on the non-adiabatic behavior of the micro-scale compressor.

RESULTS

This study begins with the analysis of the impacts of each heat flux on the global flow field at design conditions. The first analysis uses inlet air at 1 bar and 20°C. Figure 3 shows a blade-to-blade view of the temperature contours at half span, where the influence of the end-walls surface is small. Both adiabatic and diabatic walls are shown. It is interesting to note the slight temperature increase on the blades wall in the diabatic scenario. Therefore, the near-wall flow will experience a small temperature increase along the blade. The global flow field does not experience a notable change until approximately 70-80% of the streamwise location, which allows to assume an adiabatic behavior as corroborated in literature. Near the trailing edge region one can observe a slight temperature increase.

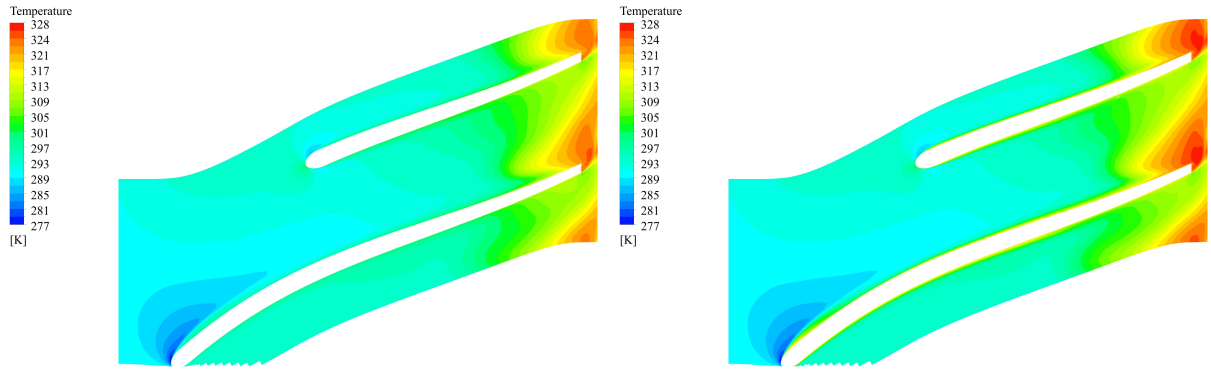

(a) Adiabatic walls (b) Diabatic walls

Figure 3: **Blade-to-blade view of temperature contours at half span.**

Another heat flux of interest is the one through the hub/shroud walls across the whole passage. Figure 4 plots the temperature profiles in the hub-to-shroud direction at 90% of the streamwise location in three different domains: inlet, impeller and diffuser. These temperature profiles are circumferentially mass-flow-averaged at the considered location and both the adiabatic and the diabatic cases are shown. One may note the small influence of the heat flux at inlet (q_1) on the global flow field. Also, the thermal boundary layer at the hub and shroud can be appreciated, where the diabatic case shows a remarkably steeper slope as expected.

Near the end of the impeller, the distorted flow due to the tip leakage phenomenon provides a temperature profile with increased temperature near the shroud. This is due to the significant entropy increase caused by that phenomenon. It can be observed how the global averaged tem-

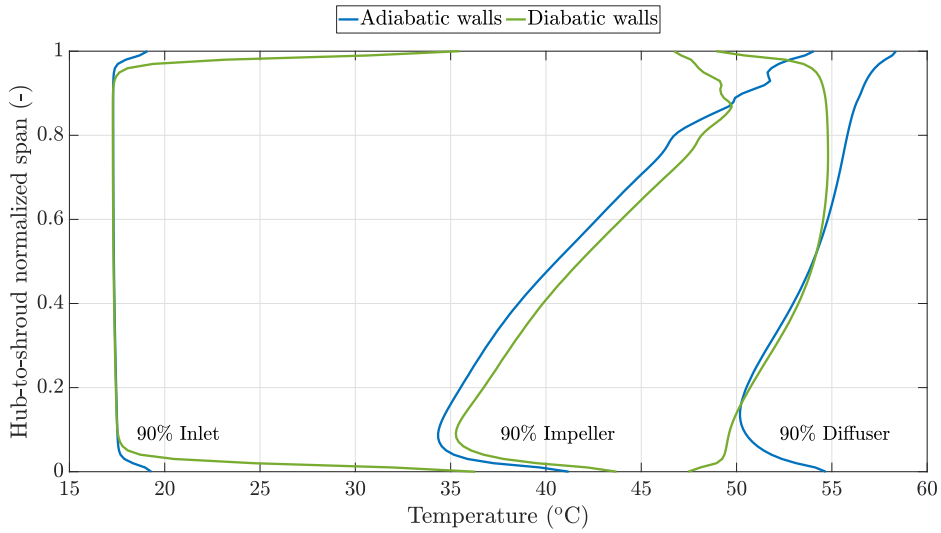

Figure 4: **Temperature profiles along the hub-to-shroud profiles at different streamwise locations for the adiabatic and diabatic case.**

perature slightly increases in the diabatic case driven by a positive net heating flux. However, it is worth noting that the heat flux on the hub and shroud have opposite directions. This is due to the different free-stream temperatures near each wall caused by the distorted flow. Because the constant wall temperature for this case is around 45°C, resultant opposite heat fluxes are provided to these two free-stream temperatures. The last profile in Figure 4 is recorded at the end of the diffuser domain. The flow is here pressurized and its temperature has increased due to the compression process. It can be appreciated that the temperature of the walls is lower than the global profile temperature. This causes a cooling flux at the hub and shroud of the diffuser.

Since a cooling flux takes place at the diffuser, another cooling stage is expected in the volute. Figures 5a and 5b show some temperature contours in different planes for the adiabatic and diabatic walls case, respectively. One may note that at this point the global flow field is completely affected by the walls, with clear differences in the entire fluid domain. These differences can be better observed in Figure 5c, where a temperature difference contour is plotted. The absolute values of the temperature differences are represented, which correspond to a cooling process through the volute. As it was expected, the larger wet surface of the volute leads to a higher heat transfer effect. However, it is true that the flow at the diffuser has a higher average velocity which may convey a higher heat transfer coefficient.

In order to compute the relative importance of each heat flux, the distribution of the studied heat fluxes is conducted below. Figure 6 shows both the computed absolute and specific heat flows at the four considered domains for four different cases: air and propane both at an inlet pressure of 1 and 4 bar. One may recall that these operating points share dynamical similarity conditions including the correspondieng Reynolds-number correction. Similarly, the selected cases have been simulated assuming diabatic walls at constant inlet-outlet mean temperature. It is interesting to observe how the two first stations correspond to heating processes while the last two stations cool the flow field, where the fluxes are notably higher. The influence of the heat flow at the impeller domain is significantly higher than the one at the inlet domain. Therefore, the specific heat flux q_1 (inlet) can be neglected. The flux at the impeller cannot be considered as negligible, but its magnitude is relatively low in comparison to the cooling fluxes in spite of

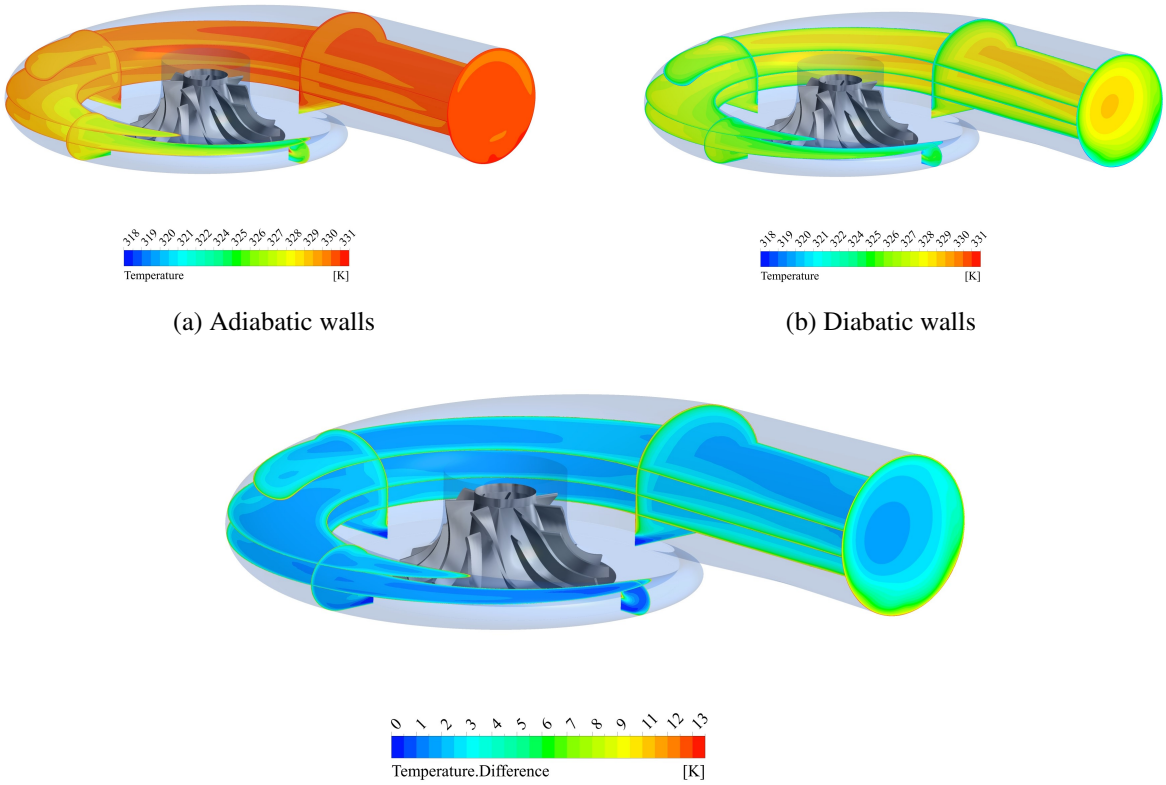

(a) Adiabatic walls

(b) Diabatic walls

(c) Difference

Figure 5: **Temperature contours at different profiles of the volute.**

the high velocity of the flow across the impeller. It can be highlighted that the volute heat flux is the largest flux considered, followed by the cooling at the diffuser with also a noteworthy importance. Therefore, it can be concluded that a global cooling is taking place when assuming diabatic walls at the averaged inlet-outlet temperature.

The trend among the different studied cases shows an increase in the absolute heat flow when pressurizing the working fluid. This occurs because an increase of the Reynolds number leads to an increase in the Nusselt number (Nu) and consequently, an increase in the heat transfer coefficient. In addition, the lower variation of the working fluid temperature lead to a higher temperature gradient with respect to the wall. Nevertheless, specific heat flux decreases when increasing inlet pressure, which results in a larger mass flows as a consequence of a higher density. This is precisely why larger turbomachines can be assumed as adiabatic.

Furthermore, the effect of changing the working fluid can be shown. Propane not only provides larger Reynolds number, which involves higher heat transfer coefficient, but it also has a lower thermal conductivity, which leads to a higher Nu. Nevertheless, it is also important to remark that these selected cases are pseudo-homologous among them. Therefore, the propane operating points require a 30% lower rotational speed to maintain the dimensional similarity. This reduced rotational speed, together with the vapor-like behavior of the propane, leads to a lower temperature increase in comparison to the cases using air: from the range of 30°C to approximately 15°C. This reduced temperature rise is responsible of the reduction of the specific heat flow when using propane, since the temperature difference at the wall is reduced by 50%.

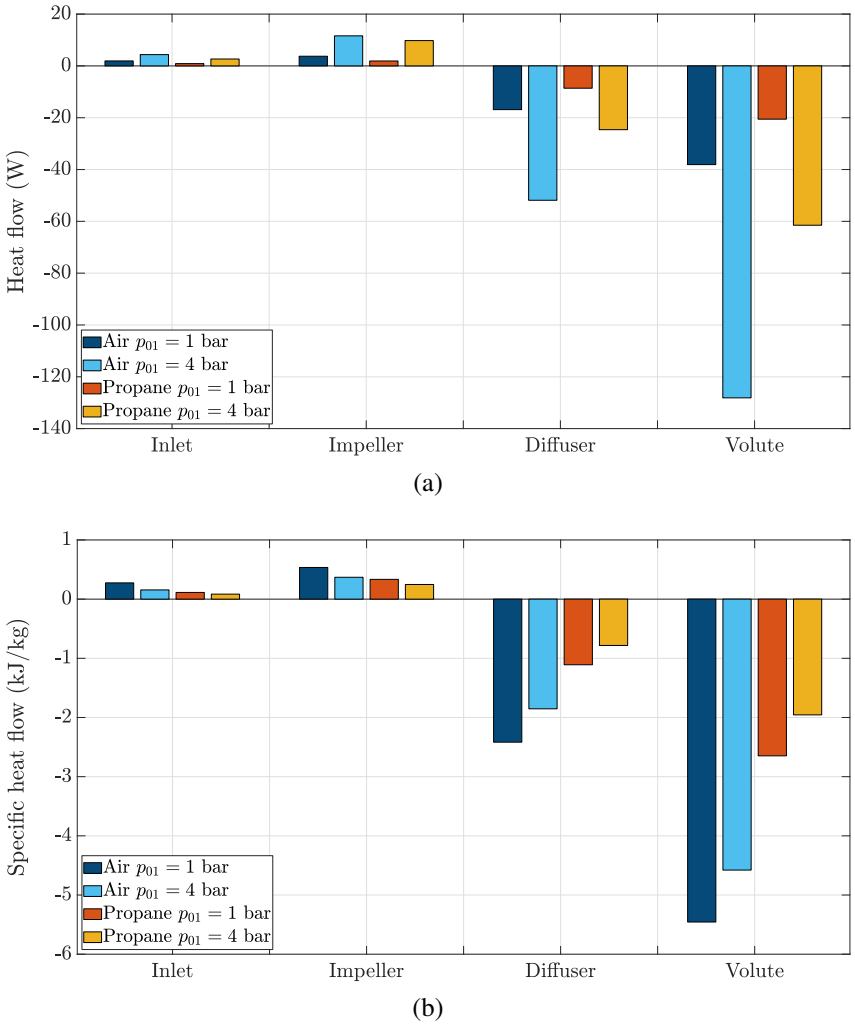

Figure 6: **Heat flows (a) and net specific heat flows (b) at the different domains for the four selected cases when considering diabatic walls.**

Finally, the effect of considering diabatic walls is analyzed across an entire speedline. Figure 7 shows the off-design performance of the full model at the design speedline using both air and propane at 1 bar (inlet conditions), which provides the lowest Reynolds number condition. Normalized pressure ratio and polytropic efficiency with their maximum value at adiabatic conditions are plotted for both the adiabatic and the diabatic (apparant) case. This latter case assumes again that the wall temperature is the averaged compressor inlet-outlet temperature. Total-to-total pressure ratio remains basically unchanged when external heat flows are being transferred to/from the flow field. This allows a straightforward experimental characterization since this parameter does not need to be corrected using neither air nor propane.

Nevertheless, the net specific heat flow has a direct impact on the polytropic efficiency of the machine. Figure 7b shows the increased effect on the apparent $\Delta\eta_p$ of the net wall heat flux at low mass flows. Furthermore, this difference is notably higher using air instead of propane due to its gas-like behavior. Hence, diabatic flows become less important when designing applications with vapor-like working fluids with lower speed of sound. In addition, higher products of speed of sound by density increase the similarity-based mass flow moving to a more adia-

batic condition. As the walls can be considered as heat sinks at the most dominant compressor domains, the apparent or diabatic polytropic efficiency is higher than the adiabatic efficiency. Otherwise, this apparent efficiency would be lower if a global heating dominates. This phenomenon makes difficult the experimental characterization of micro-scale radial compressors, particularly at low mass flow ratios. This will be further discussed in the next section. It is interesting to highlight across the selected speedline that the higher the mass flow, the more similar is the apparent efficiency to the adiabatic one, i.e. the closer is the compressor outlet temperature to the adiabatic outlet temperature.

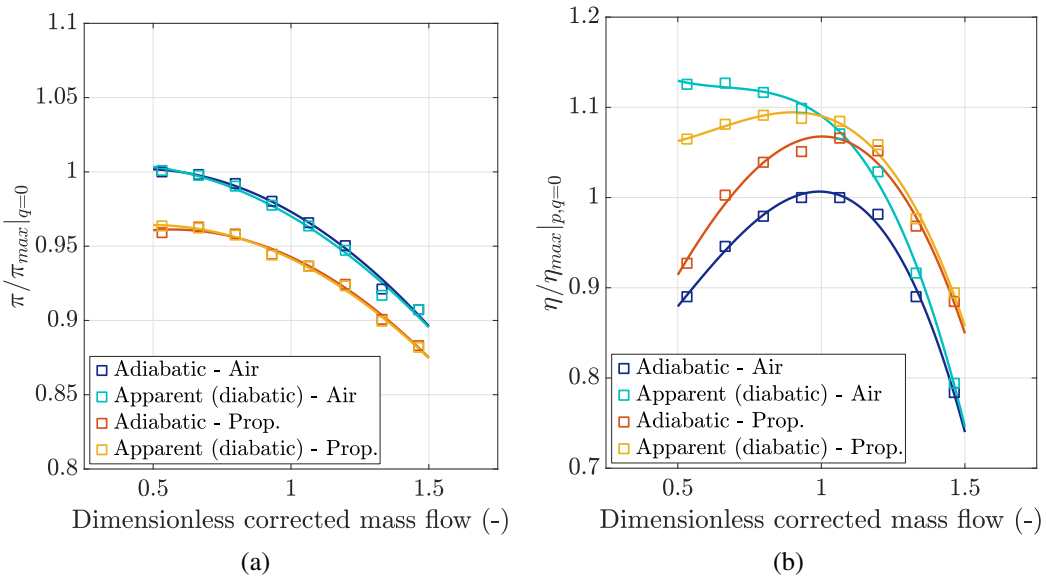

Figure 7: **Normalized (a) pressure ratio and (b) polytropic efficiency at adiabatic and diabatic conditions using air and propane (@ 1 bar) at the reference speedline.**

DISCUSSION

One of the key results obtained is the high influence of the external heat fluxes at the diffuser and the volute in comparison to the ones at the inlet and the impeller. Consequently, the heat fluxes on the blades and hub are also of lesser importance. The origin of these fluxes is the external heating/cooling of the impeller, which can occur through the axis of the machine. Since the effect of q_{2h} and q_{2b} is notably lower, one may conclude that the external flux q_{0i} is notably smaller compared to the heat fluxes on the diffuser and volute. If the external heat flux to the ambient q_{0a} is reduced with a proper thermal insulation, the only external thermal sinks/sources are both the water cooling and motor winding nodes. Therefore, one may point out that heat is mainly transferred through these two mechanisms to the compressor wall near the volute and diffuser, where a higher influence will take place. In other words, the corresponding heat addition/removal can be modeled as a post-heating/cooling once the main flow passes through the diffuser and volute.

This idea could be of great interest for the characterization of experimentally-adjusted reduced-order models for correcting the heat transfer phenomenon to generate equivalent adiabatic performances of a given micro-turbocompressor during experimental stages. Indeed, these outcomes have been experimentally applied in Sebastián et al. (2023). Complex thermal resistance networks could be simplified to a four-node star-shaped thermal resistance network,

with a central compressor wall/casing circumferentially constant temperature node. When the micro-turbocompressor casing is made of aluminum, its high thermal conductivity contributes to a more homogeneous temperature profile. Hence, a strong simplification can be made despite the complex mix of heat flows involved. Three additional nodes are required: (i) the motor winding temperature, (ii) the water cooling and (iii) the measured temperature at the compressor outlet. The net sum of the first two fluxes implies a convective heat transfer from the wall to the circulating gas/vapor across the compressor. As both the motor and the water cooling temperature could be potentially available when conducting an experimental characterization (assuming that both temperature profiles are kept axially constant), the two heat fluxes can be determined if the representative wall temperature is known. In addition, this representative node can be also predicted taking a classic heat exchanger approach on the compressor side. Therefore, a logarithmic mean temperature difference of the heat exchanger can be estimated. The resultant temperature variation can indicate how the adiabatic compressor outlet temperature turns into an apparent compressor outlet temperature.

CONCLUSIONS

The present study investigates the heat transfer issue when dealing with reduced-size radial compressors that convey to a non-adiabatic performance. The thermal particularities related to the use of high-speed electric motors instead of a conventional radial turbine have been discussed, together with their cooling needs. Therefore, the underlying mechanisms of the different resultant heat fluxes were analyzed for a reference radial compressor running with diabatic walls. This study put forward a more straight-forward heat correction methods at experimentation campaigns by means of directly correcting the heat addition/removal as a post-heating/cooling. In light of the results and discussions of this work, the following conclusions can be drawn:

- Regarding the heat flux distribution when dealing with diabatic walls at the mentioned conditions, the inlet and impeller walls have been shown to provide a very low impact on the global flow field. Nevertheless, the heat fluxes on the diffuser and, particularly, on the volute have been proven to be notably relevant. These latter heat fluxes convey a strong cooling process when an averaged inlet-outlet temperature is selected for the walls, especially at low mass flows.

- Inlet pressurization greatly reduces the impact of external heat fluxes into the flow field due to its proportional increase in mass flow. Changing the working fluid to other with higher Reynolds number and lower thermal conductivity would increase the heat transfer phenomenon. However, this can be counteracted if the given pseudo-homologous operating point results in a lower temperature rise due to lower rotational speeds.

- The apparent polytropic efficiency across a speedline can be strongly affected by the heat transfer phenomenon when dealing with diabatic flows, especially at low and medium mass flow rates. It has been proven that this issue is of greater importance when using air in comparison to propane due to is vapor-like behavior.

- The experimental characterization of micro-scale radial compressors efficiency requires to be corrected to find the apparent $\Delta\eta_p$ corresponding to the adiabatic conditions. Meanwhile, the negligible effect of the heat transfer on the resultant total-to-total pressure ratio has been proven.

- Active-cooling methods for the electric motor such as water jacket cooling and the heat delivered by the motor winding convey substantial diabatic flows on micro-compressors, particularly when dealing with non-pressurized air applications. Either those boundary conditions using very low temperature cooling water or those leaving relatively high winding temperature drastically affect the micro-compressors apparent efficiency.

ACKNOWLEDGEMENTS

This research has been supported by the Spanish *Ministerio de Ciencia e Innovación* under the project of reference number PID2019-110283RB-C32.

REFERENCES

Casey, M., Krähenbuhl, D., and Zwyssig, C. (2013). The design of ultra-high-speed miniature centrifugal compressors. In *10th European Conference on Turbomachinery, Fluid Dynamics and Thermodynamics*.

Casey, M. V. and Fesich, T. M. (2010). The Efficiency of Turbocharger Compressors With Diabatic Flows. *Journal of Engineering for Gas Turbines and Power*, 132(7). 072302.

Celik, I. B., Ghia, U., Roache, P. J., Freitas, C. J., Coleman, H., and Raad, P. E. (2008). Procedure for estimation and reporting of uncertainty due to discretization in CFD applications. *Journal of fluids Engineering-Transactions of the ASME*, 130(7):078001–078001–4.

Gong, Y., Sirakov, B. T., Epstein, A. H., and Tan, C. S. (2004). Aerothermodynamics of Micro-Turbomachinery. volume Volume 6: Turbo Expo 2004 of *Turbo Expo: Power for Land, Sea, and Air*, pages 95–102.

Kader, B. (1981). Temperature and concentration profiles in fully turbulent boundary layers. *International journal of heat and mass transfer*, 24(9):1541–1544.

Savic, B., Zimmermann, R., Jander, B., and Baar, R. (2017). New phenomenological and power-based approach for determining the heat flows of a turbocharger directly from hot gas test data. In *12th European Conference on Turbomachinery Fluid dynamics and Thermodynamics*.

Sebastián, A., Abbas, R., and Valdés, M. (2021a). Analytical prediction of reynolds-number effects on miniaturized centrifugal compressors under off-design conditions. *Energy*, 227:120477.

Sebastián, A., Abbas, R., and Valdés, M. (2021b). Effect of pressurization on tip leakage losses in micro-scale centrifugal compressors. In *14th European Conference on Turbomachinery, Fluid Dynamics and Thermodynamics*.

Sebastián, A., Abbas, R., and Valdés, M. (2023). Experimental investigation of key aerothermal phenomena in micro-scale radial turbocompressors. *Thermal Science and Engineering Progress*, 39:101748.

Sebastián, A., Abbas, R., Valdés, M., and Rovira, A. (2021c). Modular micro-trigeneration system for a novel rotatory solar fresnel collector: A design space analysis. *Energy Conversion and Management*, 227:113599.

Serrano, J. R., Olmeda, P., Arnau, F. J., Reyes-Belmonte, M. A., and Tartoussi, H. (2015). A study on the internal convection in small turbochargers. proposal of heat transfer convective coefficients. *Applied Thermal Engineering*, 89:587–599.

Sirakov, B. (2005). Characterization and design of non-adiabatic micro-compressor impeller and preliminary design of self-sustained micro engine system. *PhD Thesis, Massachusetts Institute of Technology*.

Sun, Q., Li, Q., Arshad, A., and Li, Z. (2014). Non-adiabatic flow characteristics of micro impeller. *Propulsion and Power Research*, 3(1):1–8.

Tüysüz, A., Steichen, M., Zwyssig, C., and Kolar, J. W. (2015). Advanced cooling concepts for ultra-high-speed machines. In *9th International Conference on Power Electronics and ECCE Asia*, pages 2194–2202. IEEE.

Van den Braembussche, R., Islek, A., and Alsalihi, Z. (2003). Aerothermal optimization of micro-gas turbine compressor including heat transfer. In *International Gas Turbine Congress 2003 Tokyo November 2-7, 2003*.

Verstraete, D. and Hewakuruppu, Y. (2012). Impact of Heat Transfer on Centrifugal Compressors of Micro Turbines. volume Volume 7: Fluids and Heat Transfer, Parts A, B, C, and D of *ASME International Mechanical Engineering Congress and Exposition*, pages 983–991.